PLL-Based Feed-Forward Control to Attenuate Low-Frequency Common-Mode Voltages in Transformerless LVDC Systems

Thiago R. Oliveira, *Member, IEEE*, Waner Wodson A. G. Silva, *Student Member, IEEE*, Seleme I. Seleme, Jr., and Pedro F. Donoso-Garcia

***Abstract*—Low-voltage dc distribution systems have gained significant attention over the last years, since they provide simpler and more efficient integration of distributed generators and storage devices, establishing a pathway to net zero energy buildings. In low-power units, transformerless utility interface is preferred to reduce footprint and losses. However, the lack of galvanic isolation introduces a common-mode (CM) path between the dc distribution bus and the utility service grounding, leading to the presence of high CM voltages at the dc bus feeders. The attenuation of the CM voltage reduces the touch voltage amplitude and leakage current, contributing to a safer environment. In this paper, a feed-forward active compensation of the CM voltage is proposed. It relies on utility voltage parameters, estimated by a phase locked loop, to generate a counter CM voltage; hence, it does not require previous knowledge of the system CM path model or the addition of voltage sensors. Experimental results show that this technique can attenuate the CM voltage to non-dangerous magnitudes without interfering with the microgrid differential mode behavior.**

***Index Terms*—Active control, common-mode (CM) voltage, dc power distribution, microgrids, safety.**

I. Introduction

LOW-VOLTAGE dc (LVdc) power distribution is regarded as a promising alternative to enable the development of net zero energy commercial buildings, since it promotes simpler coordination and power management of multiple distributed energy resources as well as a more efficient interface with renewables, storage, and electronic devices [1]–[5]. A LVdc microgrid is a power electronics based system, as it is shown in the basic architecture depicted in Fig. 1. The backbone of the LVdc system is a 380 V dc bus that integrates local power generation, storage system, loads, and secondary buses. The bidirectional interface with the utility grid is performed by a bidirectional grid interface converter (BGIC) and an ac/dc converter responsible for managing the power exchange between microgrid and utility, decoupling the main dc bus from utility disturbances, and ensuring grid code compliance at the point of common coupling (PCC).

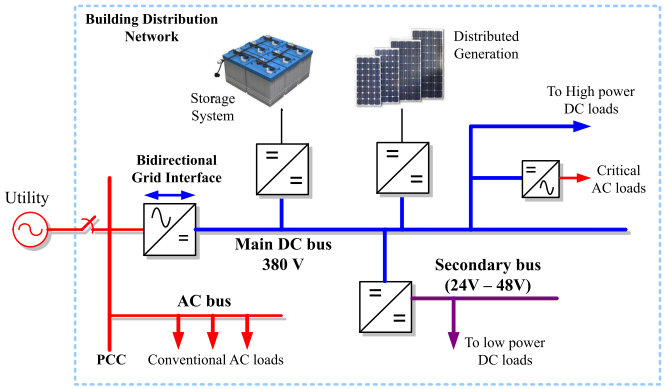

Fig. 1. Architecture of an LVdc power distribution system.

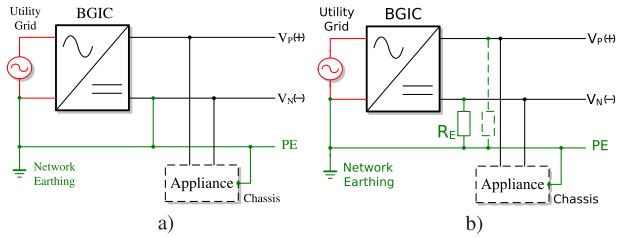

Fig. 2. LVdc grounding schemes. (a) Solidly grounded system. (b) Indirect grounded system.

In terms of safety, the behavior of the LVdc system during faults and electric shocks is highly influenced by the grounding schemes employed at the PCC and at the dc bus as well as the structure of the utility interface [6]–[8]. Commercial and residential consumers supplied by low-voltage utility distribution networks usually employ solid grounding at the building service entrance. Due to the lack of standards, the dc bus can resort to a variety of grounding methods. Fig. 2 illustrates possible solid and indirect grounding configurations for the LVdc network. As

Manuscript received September 17, 2018; revised November 21, 2018; accepted January 3, 2019. Date of publication January 7, 2019; date of current version April 20, 2019. Paper 2018-IACC-0970, presented at the 2017 Brazilian Power Electronics Conference (COBEP), Juiz de Fora, Brazil, Nov. 19–22, and approved for publication in the IEEE TRANSACTIONS ON INDUSTRY APPLICATIONS by the Industrial Automation and Control Committee of the IEEE Industry Applications Society. This work was supported by the PRPq/UFMG through the Programa Institucional de Auxílio à Pesquisa de Docentes Recém-Contratados-ADRC 01/2017. *(Corresponding author: Thiago Ribeiro Oliveira.)*

T. R. Oliveira, S. I. S., Jr., and P. F. Donoso-Garcia are with the Department of Electronic Engineering, Federal University of Minas Gerais, Belo Horizonte 31270-901, Brazil (e-mail: troliveira@cpdee.ufmg.br; seleme@cpdee.ufmg.br; pedro@cpdee.ufmg.br).

W. Wodson A. G. Silva is with the Federal University of Itajuba, Itabira 35903-087, Brazil (e-mail: waner@unifei.edu.br).

Color versions of one or more of the figures in this paper are available online at http://ieeexplore.ieee.org.

Digital Object Identifier 10.1109/TIA.2019.2891435

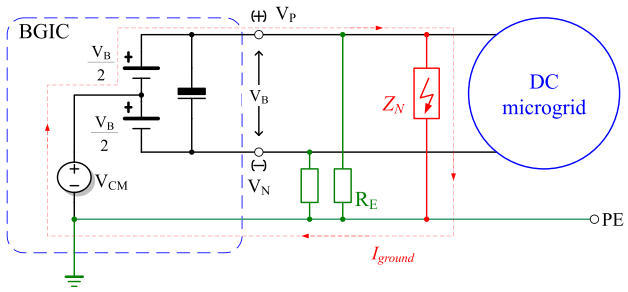

Fig. 3. Steady-state equivalent circuit of the dc bus.

both ac and dc grids are grounded, the interaction between them, in terms of leakage current, will be determined by the utility interface topology. Several proposals consider that the BGIC is endowed with an isolation transformer, which decouples both grids and enables the deployment of any grounding method at the dc side. As discussed in [9] and [10], solidly grounded microgrids will exhibit high touch voltages and low-impedance fault paths, leading to high fault and body current amplitudes. Indirect high resistance grounding (HRG), on the other hand, can limit both fault and body currents providing both continuous system operation and protection against electric shock, hence, it is the preferred choice for datacenters and other mission critical systems [11]–[13].

In low-power applications, there is no obligatory need for the employment of an isolated system, therefore transformerless LVdc distribution becomes more appealing, since it can reduce footprint and enhance efficiency [14], [15]. The lack of isolation, however, introduces a common-mode (CM) path between the ac and dc buses. In such systems, solid grounding will lead to maximum leakage current and minimum CM voltage, whilst HRG can substantially decrease the leakage current, whereas a maximum CM voltage is expected in [6] and [7].

Fig. 3 shows a steady-state equivalent circuit of the dc bus, where the dc bus voltage, regulated by the BGIC, is decomposed in its differential mode (DM) and CM terms, referred as V_B and V_{CM}, respectively, and Z_N represents a ground fault impedance or the body impedance of an electric shock victim. It can be noticed that even though HRG is employed, during ground faults or electric shocks, the current will find a path that does not encompass R_E, indicating that during grid-connected operation HRG will not be effective in reducing ground current amplitudes. Since the pole voltages can be defined as $V_{P,N} = V_{\text{CM}} \pm V_B/2$, the CM voltage will influence the magnitude of body currents during electric shocks and leakage currents induced in parasitic elements of the dc bus. Therefore, in order to provide a safer environment, the CM voltage must be eliminated.

As discussed in [6] and [16], the CM voltage in transformerless LVdc distribution systems is composed of low-frequency components, related to the utility distribution system and the BGIC dc link voltage, and high-frequency elements introduced by the converter switching pattern. In order to mitigate V_{CM}, the low- and high-frequency quantities of the CM spectrum are dealt with separately. In the literature, the elimination of the high-frequency CM components can be achieved mostly by two approaches: In the first one, additional switches can be incorporated to the BGIC topology, in order to decouple the ac and dc buses during free-wheeling stages, which are known to generate CM switching noise [17]–[19]. However, the effectiveness of the CM mitigation is not guaranteed in bidirectional operation. Another proposal, as covered in [7], [15], and [16], employs a floating filter to contain the switching noise, eliminating it from the CM spectrum of the dc bus. Such an approach is not tied to a specific converter topology, control scheme, or modulation pattern, enabling a more flexible solution to leakage current mitigation.

The elimination of the low-frequency components is attained through active control, where an intentional CM signal is introduced in the BGIC control loop in order to counter the dc bus CM voltage. In [7], an additional control loop is incorporated to a two stage BGIC converter control diagram, which measures the dc bus negative rail voltage and regulates it to -190 V through a PI + resonant compensator. The compensator output generates a CM control action that is added to the duty cycle of the converter ac/dc stage, relying on available control margin to attain CM compensation. In [15], a similar approach is presented, however, the BGIC exhibits a back-to-back topology, which enables direct elimination of the dc level of the CM voltage and allows the CM compensation to be performed by the dc/dc stage. Both proposals depend on the accurate knowledge of the microgrid CM path and parasitic elements in order to design the CM loop compensator. In [20], a feed-forward compensation is proposed, which relies only on the utility voltage measurement in order to generate a counter V_{CM} signal, dismissing the need for CM path modeling. However, this paper fails to present the impact of the proposed technique in the converter DM voltage and current waveforms, as well as its behavior in different operating conditions.

In this paper, a phase locked loop (PLL) based feed-forward active compensation of low-frequency CM voltage is proposed, which does not require previous knowledge of the LVdc system CM path transfer function or any additional voltage sensor. The remainder of the paper is organized as follows. Section II presents the utility interface architecture considered in this paper and discusses the influence of the utility network and the BGIC control on the CM voltage spectrum. Section III introduces the proposed CM active compensation technique. Section IV shows the experimental results and Section V provides the paper conclusions.

II. Utility Interface Architecture

As previously discussed, the composition of the CM spectrum is dependent on the available utility distribution configuration, the BGIC topology, and the grounding scheme employed at the PCC and at the dc bus. Therefore, it is important to establish an utility interface architecture upon which the discussions proposed in this paper can be based. Fig. 4 illustrates the proposed utility interface. It is assumed that the utility entrance is solidly grounded at the PCC and that the dc bus uses HRG in order to reduce leakage currents. A two-wire unipolar LVdc distribution is considered, instead of a bipolar three-wire system, since it does not require the employment of voltage balancers

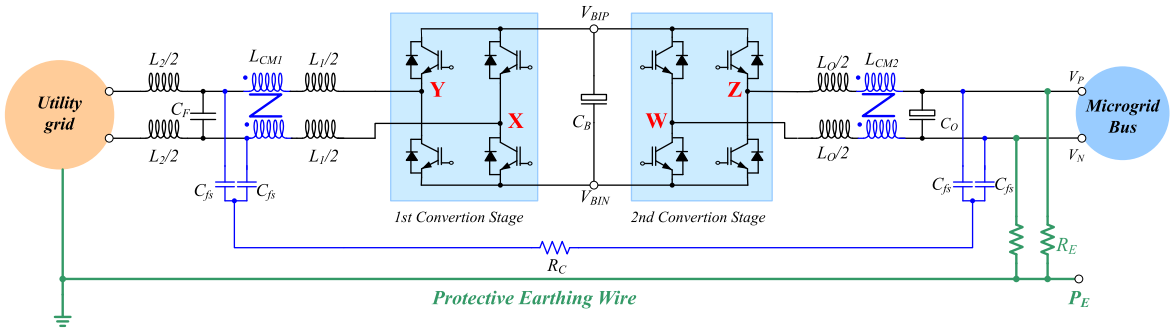

Fig. 4. BGIC topology.

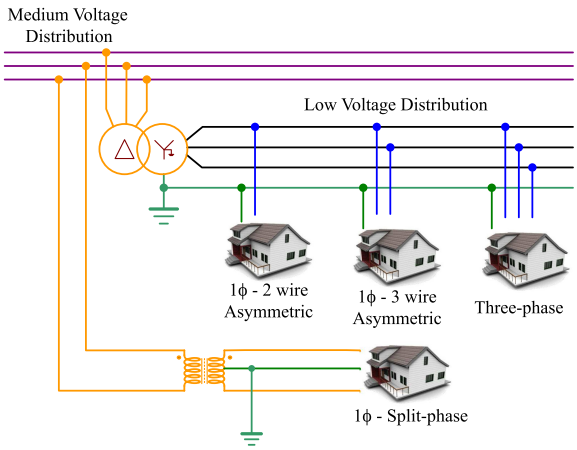

Fig. 5. Low-voltage distribution systems topologies.

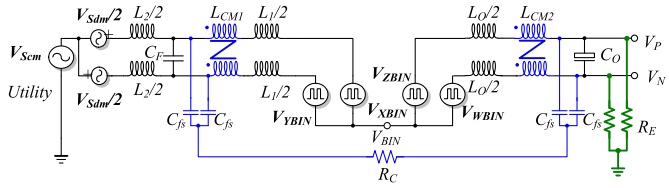

Fig. 6. Voltage source representation of the utility interface.

TABLE I
DM AND CM TERMS OF THE UTILITY VOLTAGE

Distribution	DM	CM
Split-phase	$V_m cos(\omega t)$	0
2 wire asymmetric	$V_m cos(\omega t)$	$\frac{1}{2}V_m cos(\omega t)$
3 wire asymmetric	$\sqrt{3}V_m cos\left(\omega t - \frac{\pi}{6}\right)$	$\frac{1}{2}V_m cos\left(\omega t - \frac{\pi}{3}\right)$

to deal with uneven load distribution between the feeders. A two-stage back-to-back topology is considered for the BGIC, which, although less efficient than a single-stage converter, enables current limiting at both ac and dc terminals, second harmonic ripple decoupling, and dc link capacitance reduction [21]. Moreover, it provides sufficient dc link voltage margin to incorporate CM active control strategies without compromising the utility current and dc bus voltage controls [15]. A floating filter, composed by the coupled inductors L_{CM1} and L_{CM2}, the capacitors C_{fs}, and damping resistor R_C, is used to eliminate the CM voltage switching noise.

The utility distribution service can be available in mostly four structures, as illustrated in Fig. 5. Three-phase systems are normally associated with high-power consumers, whereas, low-power residential and commercial facilities will be connected to single-phase distribution. In North America, the most common single-phase utility distribution is the split-phase system, in which a single-phase transformer with grounded secondary central tap services consumers with an 110 V/220 V three-wire system. In countries such as Brazil and China, two or more phases of a three-phase transformer are derived to supply consumers, producing asymmetric single-phase systems with two or three wires. In Brazil, for instance, a two-wire single-phase system is dedicated to consumers with installed capacity of 10 kW or lower, three-wire systems are employed to consumers with installed capacities between 10 and 15 kW, and three-phase systems are associated with consumers with capacities above 15 kW. Voltage levels can be either 127 V/220 V or 220 V/380 V, depending on the region. As this paper focuses in transformerless low-power LVdc systems, only single-phase distribution will be considered henceforward.

A. CM Voltage Composition

In order to quantify the CM quantities of the LVdc system described above, a voltage source representation of the BGIC and the utility distribution system, as shown in Fig. 6, was considered. It decomposes the utility grid voltage in its DM ($V_{S\text{dm}}$) and CM ($V_{S\text{cm}}$) terms and replaces the BGIC switching legs with voltage sources V_{XBIN}, V_{YBIN}, V_{ZBIN}, and V_{WBIN}.

The utility DM and CM voltages will be influenced by the available utility distribution service. Assuming that the phase-to-neutral voltages can be expressed as $V_{\text{phase}} = V_m \cos(\omega t + \theta)$, where V_m is the phase peak voltage, ω is the grid angular frequency, and θ is the angular displacement; the DM and CM terms of the utility voltage will be as given in Table I.

It can be observed that the symmetry of a split-phase distribution leads to approximately zero CM voltage contribution. In a real situation, a small CM voltage is expected due to mismatches between the distribution transformer secondary windings. In two or three wire asymmetric distribution, a CM voltage with half the phase voltage amplitude will appear at the dc bus.

Regarding the BGIC switching pattern, unipolar pulsewidth modulation (PWM) is widely employed in full-bridge converters, since it allows filter size reduction, when compared to bipo-

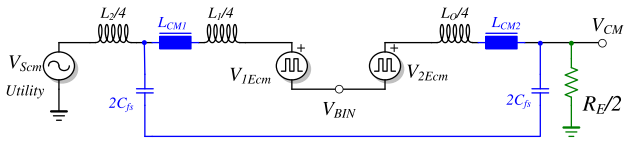

Fig. 7. CM model of the dc bus.

lar modulation. Assuming that unipolar PWM is used in both stages, each switching leg voltage can be described as

$$V_{jBIN} = D_j v_{BI} + H_{F\text{pwm},j} \tag{1}$$

where $j = [X, Y, W, Z]$, $v_{BI} = V_{BI} + \Delta v_{BI}$ is the dc link voltage with an 120 Hz ripple, D_j is the switching leg duty cycle and $H_{F\text{pwm},j}$ are the switching frequency harmonics and interharmonics. The duty cycle can be defined as

$$D_j = \frac{1}{2}\left(1 + d_j / V_{\text{tri}}\right) \tag{2}$$

where d_j is the jth leg control action and V_{tri} is the triangular carrier peak voltage. The voltage sources can be combined to extract the DM and CM contributions of each stage, where $V_{1E\text{dm}} = V_{XBIN} - V_{YBIN}$ and $V_{2E\text{dm}} = V_{ZBIN} - V_{WBIN}$ are the DM terms of the first and second stage, respectively, and $V_{1E\text{cm}} = 0.5(V_{YBIN} + V_{XBIN})$ and $V_{2E\text{dm}} = 0.5(V_{ZBIN} + V_{WBIN})$ are the CM terms. As the unipolar PWM establishes that $d_x = -d_y$ and $d_z = -d_w$, the CM contributions of each stage will become

$$V_{1E\text{cm}} = \frac{1}{2} \cdot v_{BI} + H_{F\text{pwm1}} \tag{3}$$

$$V_{2E\text{cm}} = \frac{1}{2} \cdot v_{BI} + H_{F\text{pwm2}} \tag{4}$$

where $H_{F\text{pwm1}}$ is a combination of the high-frequency components of legs X and Y and $H_{F\text{pwm2}}$ is the same for legs W and Z. Since the utility grid and BGIC contributions to the dc system CM voltage are known, a CM model of the dc bus can be defined, as shown in Fig. 7.

Through the CM model, the dc bus CM voltage (V_{CM}) can be expressed as

$$V_{\text{CM}} = \frac{R_E}{sL_2/2 + R_E}(V_{S\text{cm}} + V_{I\text{cm}}(s)) \tag{5}$$

where $V_{I\text{cm}}(s)$ is the BGIC equivalent CM voltage, which is defined as

$$V_{I\text{cm}}(s) = \frac{(2sC_{fs}R_C + 1) \cdot (V_{1E\text{cm}} - V_{2E\text{cm}})}{2s^2 C_{fs} L_{\text{eq}} + 2sC_{fs}R_C + 1} \tag{6}$$

where $L_{\text{eq}} = L_{\text{CM1}} + L_{\text{CM2}} + L_1/4 + L_O/4$. It is important to highlight that as $V_{1E\text{cm}} - V_{2E\text{cm}} = H_{F\text{pwm1}} - H_{F\text{pwm2}}$, the BGIC switching legs will only contribute with high-frequency noise to the system CM voltage, i.e., the dc component is naturally eliminated by the unipolar PWM. As the floating filter has a low-pass behavior, its elements can be designed to attenuate the switching noise to desired levels. In [16], a design procedure for floating filters is described, which advises the use of small C_{fs} capacitances, leaving the responsibility of suppressing the CM switching voltage to the coupled inductors, hence a very small current will flow through the capacitive loop, requiring small damping resistance. Assuming that R_C is quite small, the filter cut-off frequency can be defined as

$$\omega_c \approx \sqrt{\frac{1}{\left(\frac{L_1}{4} + \frac{L_O}{4} + L_{\text{CM1}} + L_{\text{CM2}}\right) 2C_{fs}}} \tag{7}$$

which promotes an attenuation of $20\log_{10}|1 - (\omega/\omega_c)^2|$. This relationship can be used to impose the desired attenuation to the BGIC switching noise.

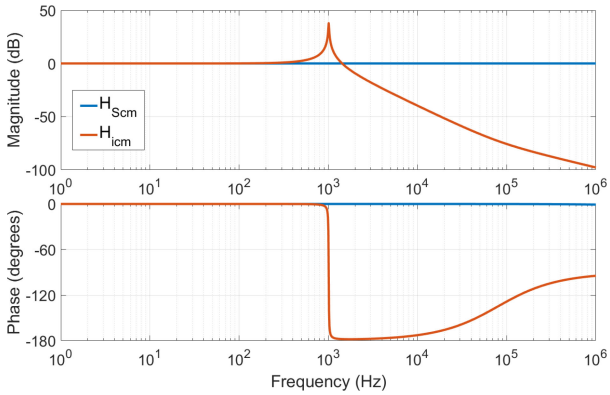

Fig. 8. CM transfer functions.

The system CM transfer functions can be defined, through (5) and (6), as

$$H_{S\text{cm}} = \frac{R_E}{sL_2/2 + R_E} \tag{8}$$

$$H_{i\text{cm}} = \frac{R_E(2sC_{fs}R_C + 1)}{(2s^2 C_{fs} L_{\text{eq}} + 2sC_{fs}R_C + 1)(sL_2/2 + R_E)} \tag{9}$$

where $H_{S\text{cm}}(s) = V_{\text{CM}}/V_{S\text{cm}}$ and $H_{i\text{cm}} = V_{\text{CM}}/(V_{1E\text{cm}} - V_{2E\text{cm}})$. In order to generate neglectful leakage current, the grounding resistance R_E is usually very high, a few tens of kΩ, which allocates the pole of $H_{S\text{cm}}$ near the MHz range. Since the grid voltage spectrum lies in the low-frequency region, the transfer function can be approximated as $H_{S\text{cm}} \approx 1$, i.e., the low-frequency components of the CM voltage will be exactly $V_{S\text{cm}}$. Therefore, V_{CM} can be simplified as

$$V_{\text{cm}}(s) \approx V_{S\text{cm}} + \frac{(2sC_{fs}R_C + 1)(V_{1E\text{cm}} - V_{2E\text{cm}})}{2s^2 C_{fs} L_{\text{eq}} + 2sC_{fs}R_C + 1}. \tag{10}$$

As an example, Fig. 8 shows the CM transfer functions for a LVdc system employing a 5 kW BGIC, which interfaces an asymmetric utility distribution with 127 V phase voltage and a 380 V dc bus, grounded through 22 kΩ resistances. The floating filter was designed to attenuate 50 dB at the switching frequency, which is set as 15.36 kHz. The system parameters were the same as used in the experimental platform and will be fully described in Section IV.

It can be noticed that, for the region of interest, $H_{S\text{cm}}$ equals 0 dB. $H_{i\text{cm}}$ presents a second-order low-pass filter behavior, with a resonance frequency at 1 kHz, providing the designed attenuation at 15.36 kHz. Fig. 9 shows the simulated CM voltage waveform and fast Fourier transform for the BGIC described

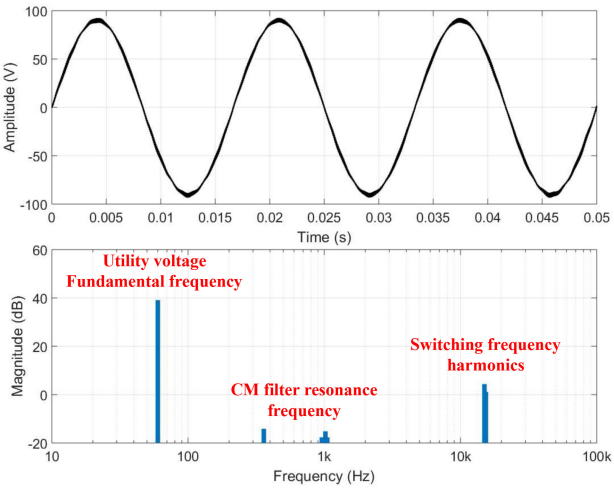

Fig. 9. Simulated CM voltage waveform and spectrum.

above. The line frequency component is half the grid phase voltage, i.e., 63.5 Vrms (90 V peak–39 dB) and the CM spectrum also presents attenuated components at the filter resonance frequency and at the switching frequency.

Since $H_{i\mathrm{cm}} = 1\angle 0^\circ$ for the line frequency range, this example indicates that if a CM control action is incorporated at the BGIC duty cycle, $V_{1E\mathrm{cm}}$ or $V_{2E\mathrm{cm}}$ can be used to compensate $V_{S\mathrm{cm}}$ and attenuate the line frequency component of V_{CM}.

III. Low-Frequency CM Voltage Compensation

The proposed BGIC with floating filter is able to attenuate high-frequency noise present in the CM voltage spectrum, however, the CM transfer function for the utility grid voltage has an unitary gain in the line frequency range, meaning that the grid CM voltage will directly appear at the dc bus. The elimination of the low-frequency CM components can be performed through active control of the BGIC, adding a counter CM component in the $V_{i\mathrm{cm}}$ term, which will compensate the existence of the grid CM voltage. In this paper, the CM compensation will be introduced in the second-stage (dc/dc) control loop, in order to not to interfere with the utility grid current control, which is performed by the first stage (ac/dc).

The proposed technique assumes that the LVdc system has insignificant influence on the utility voltage; therefore, the utility CM component will only depend on the utility conditions, hence, if the PCC characteristics are monitored, $V_{S\mathrm{cm}}$ can be estimated by the BGIC. As most utility interface converters employ a PLL to synchronize the converter output ac current with the utility voltage, achieving unity power factor, this structure can be used to gather information concerning the PCC voltage and frequency conditions. Therefore, as long as the PLL algorithm is able to estimate the PCC amplitude and frequency, a proper CM compensation signal can be generated and added to the converter control loop. Thus, a synchronous reference frame PLL, as described in [22], was employed in this paper. The PLL diagram is depicted in Fig. 10, where potential difference is the phase detector block, V_S is the normalized utility voltage, $\hat{\theta}$ is the estimated phase, and $\hat{\omega_o}$ is the estimated utility frequency.

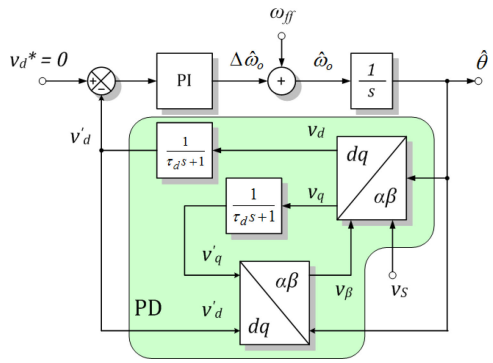

Fig. 10. Synchronous reference frame PLL.

The PLL performs a park transformation, using the utility voltage as the input α-axis and generating the β-axis. When the phase is locked, the internal d-axis will be regulated to zero and V_β will be orthogonal to V_S. In this moment, the q-axis will be equal to the utility peak voltage. Since V_S is normalized, V_q' will be in p.u.

The proposed CM compensation diagram is shown in Fig. 11, where a CM control action (d_{cm}) is fed forward to the second-stage PWM modulator. The DM control diagram employs conventional cascaded voltage and current control loops to track the grid current waveform and regulate the dc link and dc bus voltages, therefore, it is not detailed in the figure.

The CM control action d_{cm} is defined as

$$d_{\mathrm{cm}} = \frac{k_{\mathrm{cm}} v_{qu}}{v_{BI}} \cos(\omega t + \varphi) \tag{11}$$

where v_{qu} and ωt are PLL outputs representing the utility normalized peak voltage and its angular displacement respectively, φ is a predefined phase angle, and k_{cm} is a gain. The resulting CM signal can be calculated as

$$V^*_{I\mathrm{cm}} = \frac{d_{\mathrm{cm}}}{2V_{\mathrm{tri}}} v_{BI}. \tag{12}$$

Assuming an 127 Vrms phase-to-neutral voltage and forcing $V^*_{I\mathrm{cm}} = V_{s\mathrm{cm}}$, through (12) and the grid CM term given in Table I, the parameters k_{cm} and φ for all three single-phase distribution systems can be calculated, which is given in Table II. It is important to mention that the displacement φ shown for a Three-wire asymmetric system was calculated assuming a phase-to-phase grid voltage measurement, which adds a $\pi/6$ displacement to the one given in Table I.

A. Proposed Technique Limitations

Since the CM compensation signal is added to the BGIC DM control signals of each second-stage switching leg, the resulting leg duty cycle must be designed to prevent the saturation of the dc/dc stage. According to (2), taking leg Z as an example, the average voltage V_{ZBIN} can be calculated as

$$V_{ZBIN} = \frac{1}{2}\left(1 + \frac{d_{zw} - d_{\mathrm{cm}}}{V_{\mathrm{tri}}}\right) V_{BI} \tag{13}$$

where d_{zw} is the differential control signal for the BGIC second stage. Since the DM mode imposes that $d_{zw} V_{BI}/V_{\mathrm{tri}} = V_B$, the

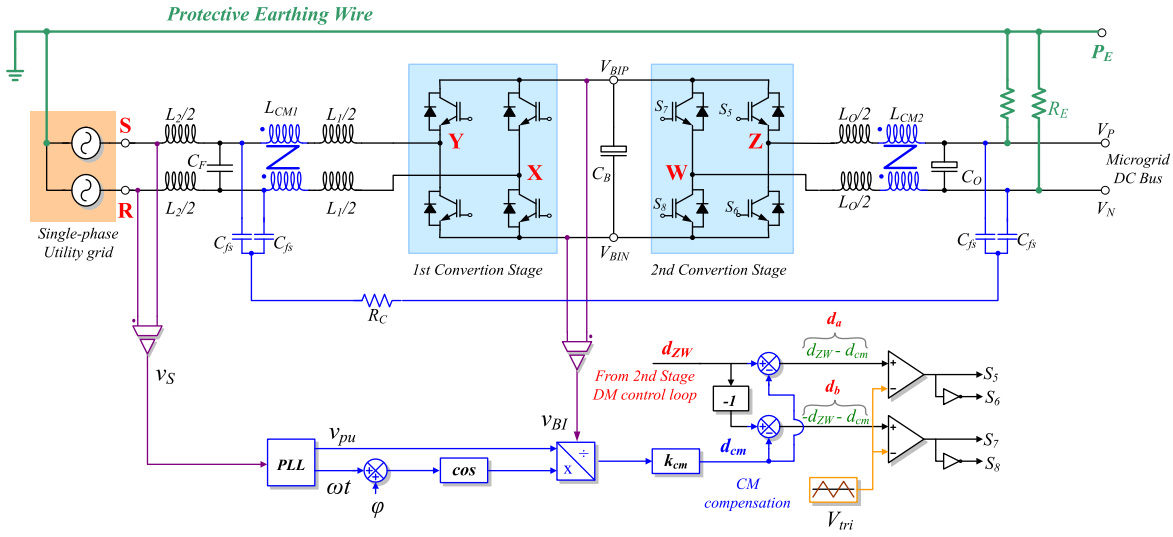

Fig. 11. Low-frequency CM voltage compensation.

TABLE II
CM COMPENSATION PARAMETERS

Distribution	k_{cm}	φ
Split-phase	0	0
2 wire asym.	$180V \cdot V_{tri}$	0
3 wire asym.	$180V \cdot V_{tri}$	$-\pi/2$

switching leg voltage can be redefined as

$$V_{ZBIN} = \frac{V_{BI}}{2} + \frac{V_B}{2} - V^*_{\mathrm{Icm}}. \tag{14}$$

The maximum voltage that a switching leg can impose is equal to the dc link voltage (V_{BI}), hence, from (14) it can be established that

$$V_{BI\min} > V_{B\max} + V_m \tag{15}$$

where $V_{B\max}$ is the microgrid dc bus maximum allowed voltage and $V_{BI\min}$ is the minimum allowed dc link voltage. If relationship (15) is satisfied, the grid converter will be able to perform the CM voltage compensation and the dc bus voltage control without PWM overmodulation.

Moreover, since the proposed technique is an open-loop method, the elimination of the CM voltage relies on the BGIC ability to reproduce the utility CM contribution waveform. Therefore, in order to achieve complete mitigation of the CM low-frequency components, the PLL algorithm must be able to precisely estimate the amplitude and phase of all relevant harmonics of the utility voltage and the dc/dc stage must be able to accurately synthesize them as well. Those conditions, in practice, are impossible due to the precision of voltage sensors, errors introduced by any digital implementation of the PLL algorithm, errors introduced by deadtime in the power converter, etc. Thus, another limitation of the proposed technique is that it can attenuate the magnitude of the CM voltage, however, it is unable to attain complete CM voltage mitigation.

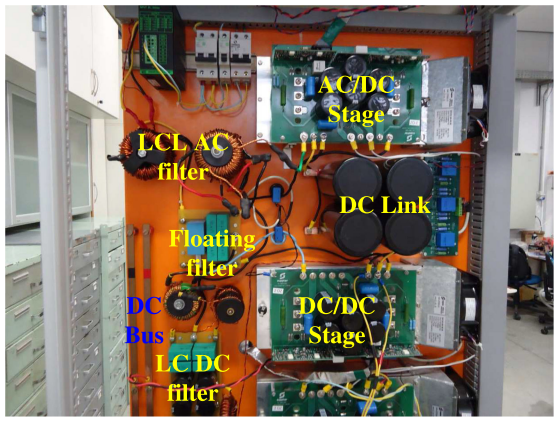

Fig. 12. Experimental setup.

TABLE III
BGIC CONVERTER FILTER VALUES

Elements	Value	Elements	Value
L_1	360μH	C_O	470μF
L_2	100μH	L_{CM1}	9mH
L_O	1.3mH	L_{CM2}	3mH
C_f	20μF	C_{fs}	1μF
R_E	22kΩ	R_C	1Ω

IV. EXPERIMENTAL RESULTS

The behavior of the proposed CM compensation was assessed through a 5 kW experimental setup, shown in Fig. 12. The converter is connected to a three-wire asymmetric utility distribution, with 127 V/220 V voltage levels, as shown in Fig. 11. The dc bus nominal voltage is 380 V, hence, in order to satisfy (15), the minimum dc link voltage should be 560 V. A 600 V $\pm$ 2% dc link was chosen for this prototype. The switching frequency was set as 15.36 kHz. The DM and floating CM filter values are given in Table III, where the cut-off frequency of the floating filter was calculated to provide a 50 dB attenuation at the

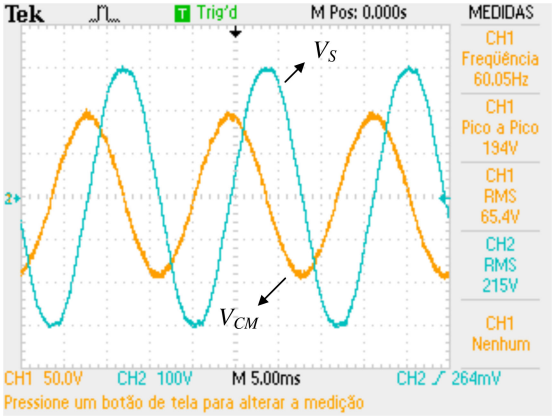

Fig. 13. Grid line voltage and CM voltage waveforms.

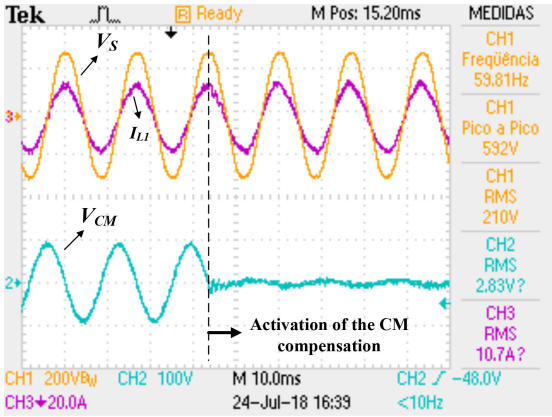

Fig. 14. Grid voltage and current response to CM compensation.

switching frequency. The system transfer functions are the same as the ones previously shown in Fig. 8.

Fig. 13 shows the measured utility line voltage and the CM voltage at the dc bus. The CM voltage amplitude is 65.4 Vrms, about half the utility phase voltage, and a 90° displacement can be seen between it and the grid line voltage. As previously discussed, the CM voltage should exhibit a $\pi/3$ displacement in relation to the grid phase voltage in a three-wire asymmetric system; therefore, in relation to the line voltage, an extra $\pi/6$ displacement is introduced, resulting in a $\pi/2$ total displacement as observed.

A. *Response to the Activation of CM Compensation*

Fig. 14 shows the behavior of the PCC quantities when the CM compensation is activated. The BGIC imports 2.4 kW from the utility with unity power factor. It can be observed that the CM compensation substantially reduces the CM voltage magnitude instantly after the beginning of the active CM control. However, its impact on the grid variables in steady state is unnoticeable. The spectra of the grid current and CM voltage before and after the activation of the CM compensation strategy are shown in Figs. 15 and 16, respectively.

It can be observed that CM compensation has some influence over the grid current harmonic spectrum. The odd harmonics

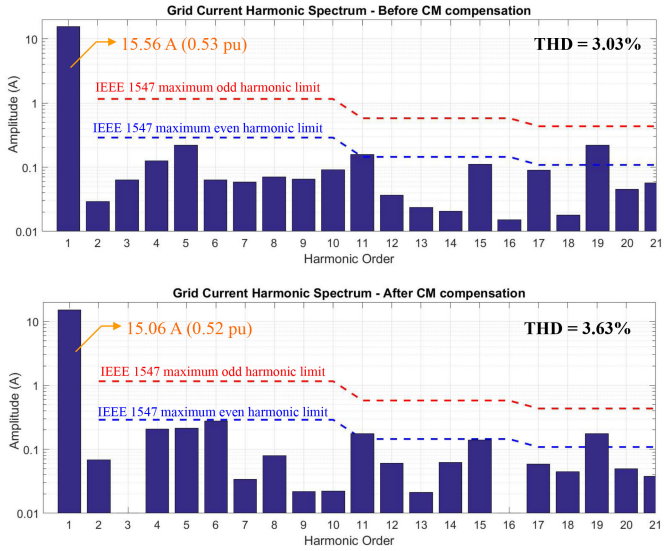

Fig. 15. Harmonic spectrum of the grid current.

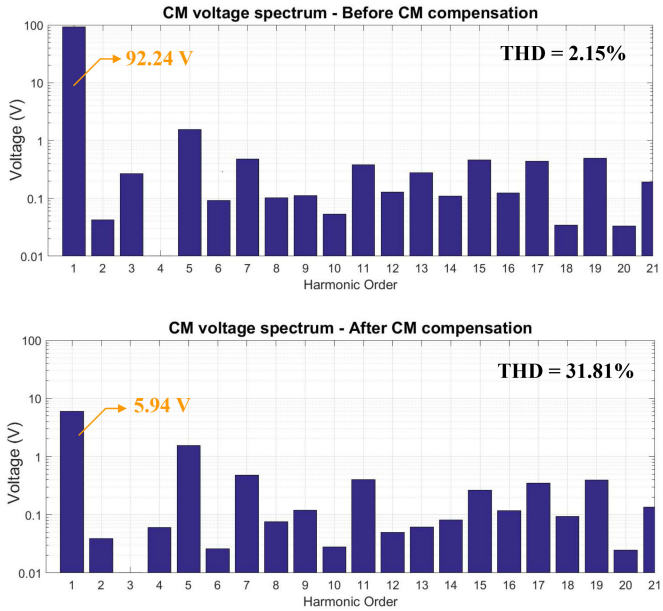

Fig. 16. CM voltage spectrum before and after compensation.

are either unaltered or are slightly decreased after the CM compensation has been activated, whereas the even harmonics are mostly increased, which raises the current total harmonic distortion (THD) from 3.03% to 3.63%. However, the individual harmonics and total harmonic distortion lie below the IEEE 1547 requirements, thus compliance with grid connection standards is not compromised. The reason for this increase is that a small 60 Hz current is supplied by the BGIC dc side to the dc bus CM circuit, introducing 60 Hz ripple in the dc link. The interaction of first and second harmonic ripples in the dc link with the DM grid current control loop generates residual even harmonics in the current spectrum. Regarding the CM voltage spectrum, the original signal exhibits relatively high third and seventh harmonics, which are related to the available grid voltage in the laboratory. After the activation of the CM compensation, the

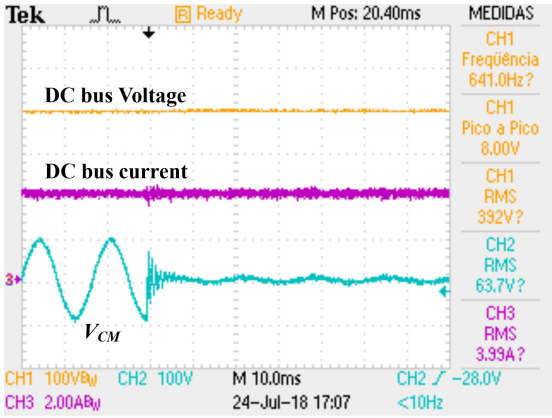

Fig. 17. CM compensation impact on the dc bus.

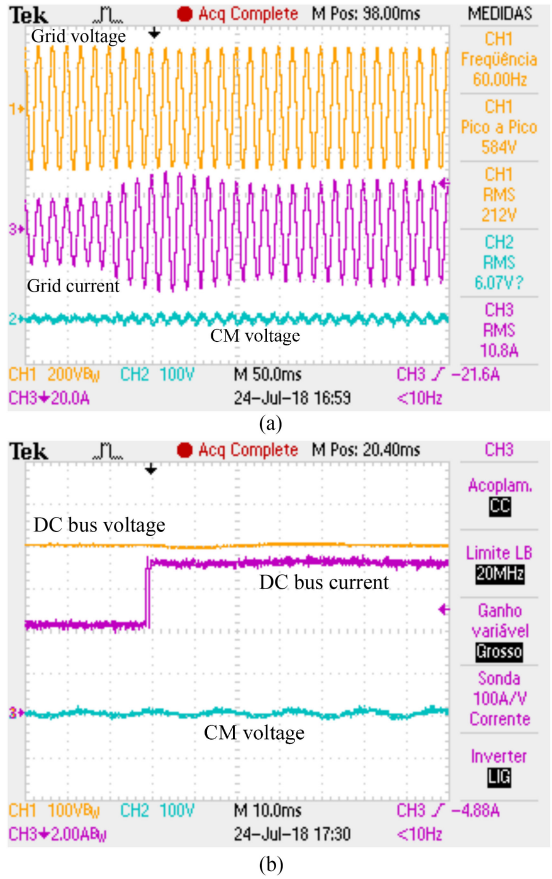

Fig. 18. System response to load step. (a) AC grid. (b) DC bus.

CM voltage fundamental component amplitude was attenuated 23.8 dB, from 92.24 to 5.94 V. However, the technique had a mild effect on the CM voltage harmonic content. This is due to the fact that the CM control action is derived from the PLL output signals, which, in this paper, only accounts for the grid voltage fundamental component. A greater attenuation of the CM voltage is hampered by voltage measurement accuracy and errors in the PLL estimation of the grid voltage amplitude. The CM compensation impact on the dc bus is shown in Fig. 17, for the same load scenario. It indicates that the dc bus voltage and current are also not significantly influenced by the CM active control.

B. System Response to a Load Step

Fig. 18 shows the behavior of the system during a load step increase from 50% to 80%. It can be observed that the DM control was able to regulate the dc bus voltage accordingly and manage the power exchange between the BGIC and the utility grid, therefore, the feed-forward CM compensation did not compromise the BGIC operation. On the other hand, the output power increase and the variation of the grid current and dc bus voltage were transparent to the compensated CM voltage, showing that the proposed feed-forward compensation is effective in attenuating the LVdc system CM low-frequency components, independently on the system operation.

V. Conclusion

This paper proposed a PLL-based feed-forward active compensation of CM low-frequency components in LVdc systems. The technique is not model based, i.e., it does not require previous knowledge of the LVdc CM path to promote CM voltage attenuation, and no additional voltage sensor is needed. It relies on utility voltage and frequency estimations, provided by the interface converter PLL, to generate a CM control action at the converter dc bus side that will be able to attenuate the system CM voltage. Experimental results show that the proposed technique is able to attenuate the CM voltage in 23 dB with deadbeat response. The compensation has also shown little interference with the utility interface converter DM control objectives, i.e., grid current control and dc bus regulation. Moreover, the CM compensation is robust to shifts in the operation point of the converter.

References

[1] D. J. Becker and B. J. Sonnenberg, "DC microgrids in buildings and data centers," in *Proc. IEEE 33rd Int. Telecommun. Energy Conf.*, 2011, pp. 1–7.

[2] R. Weiss, L. Ott, and U. Boeke, "Energy efficient low-voltage DC-grids for commercial buildings," in *Proc. IEEE 1st Int. Conf. DC Microgrids*, Jun. 2015, pp. 154–158.

[3] M. Ton, B. Fortenbery, and W. Tschudi, "DC power for improved data center efficiency," , Lawrence Berkeley Nat. Lab., Berkeley, CA, USA, Tech. Rep., 2007. [Online]. Available: http://energy.lbl.gov/ea/mills/HT/documents/data_centers/ DCDemoFinalReportJan17-07.pdf

[4] D. Salomonsson and A. Sannino, "Low-voltage DC distribution system for commercial power systems with sensitive electronic loads," *IEEE Trans. Power Del.*, vol. 22, no. 3, pp. 1620–1627, Jul. 2007.

[5] A. Sannino, G. Postiglione, and M. H. J. Bollen, "Feasibility of a DC network for commercial facilities," *IEEE Trans. Ind. Appl.*, vol. 39, no. 5, pp. 1499–1507, Sep./Oct. 2003.

[6] T. R. Oliveira, A. S. Bolzon, and P. F. Donoso-Garcia, "Grounding and safety considerations for residential DC microgrids," in *Proc. 40th Annu. Conf. IEEE Ind. Electron. Soc.*, Oct. 2014, pp. 5526–5532.

[7] F. Chen, R. Burgos, D. Boroyevich, and X. Zhang, "Low-frequency common-mode voltage control for systems interconnected with power converters," *IEEE Trans. Ind. Electron.*, vol. 64, no. 1, pp. 873–882, Jan. 2017.

[8] T. Dragicevic, X. Lu, J. Vasquez, and J. Guerrero, "DC microgrids–Part II: A review of power architectures, applications, and standardization issues," *IEEE Trans. Power Electron.*, vol. 31, no. 5, pp. 3528–3549, May 2016.

[9] D. Kumar, F. Zare, and A. Ghosh, "DC microgrid technology: System architectures, AC grid interfaces, grounding schemes, power quality, communication networks, applications, and standardizations aspects," *IEEE Access*, vol. 5, pp. 12 230–12 256, 2017.
[10] N. Bayati, A. Hajizadeh, and M. Soltani, "Protection in DC microgrids: A comparative review," *IET Smart Grid*, vol. 1, no. 3, pp. 66–75, Oct. 2018.
[11] K. Hirose *et al.*, "Grounding concept considerations and recommendations for 400VDC distribution system," in *Proc. IEEE 33rd Int. Telecommun. Energy Conf.*, 2011, pp. 1–8.
[12] M. Noritake, T. lino, A. Fukui, K. Hirose, and M. Yamasaki, "A study of the safety of the DC 400 V distribution system," in *Proc. IEEE 31st Int. Telecommun. Energy Conf.*, 2009, pp. 1–8.
[13] S. Beheshtaein, M. Savaghebi, J. C. Vasquez, and J. M. Guerrero, "Protection of AC and DC microgrids: Challenges, solutions and future trends," in *Proc. IECON 41st Annu. Conf. IEEE Ind. Electron. Soc.*, Nov. 2015, pp. 005253–005260.
[14] M. Mobarrez, D. Fregosi, S. Bhattacharya, and M. A. Bahmani, "Grounding architectures for enabling ground fault ride-through capability in DC microgrids," in *Proc. IEEE 2nd Int. Conf. DC Microgrids*, Jun. 2017, pp. 81–87.
[15] F. Chen, R. Burgos, and D. Boroyevich, "A bidirectional high-efficiency transformerless converter with common-mode decoupling for the interconnection of AC and DC grids," *IEEE Trans. Power Electron.*, vol. 34, no. 2, pp. 1317–1333, Feb. 2019.
[16] D. Dong, F. Luo, D. Boroyevich, and P. Mattavelli, "Leakage current reduction in a single-phase bidirectional AC-DC full-bridge inverter," *IEEE Trans. Power Electron.*, vol. 27, no. 10, pp. 4281–4291, Oct. 2012.
[17] S. V. Araujo, P. Zacharias, and R. Mallwitz, "Highly efficient single-phase transformerless inverters for grid-connected photovoltaic systems," *IEEE Trans. Ind. Electron.*, vol. 57, no. 9, pp. 3118–3128, Sep. 2010.
[18] B. Ji, J. Wang, and J. Zhao, "High-efficiency single-phase transformerless PV H6 inverter with hybrid modulation method," *IEEE Trans. Ind. Electron.*, vol. 60, no. 5, pp. 2104–2115, May 2013.
[19] R. Gonzalez, J. Lopez, P. Sanchis, and L. Marroyo, "Transformerless inverter for single-phase photovoltaic systems," *IEEE Trans. Power Electron.*, vol. 22, no. 2, pp. 693–697, Mar. 2007.
[20] T. R. Oliveira, S. I. Seleme, and P. F. Donoso-Garcia, "Feed-forward active attenuation of low frequency common-mode voltages in DC microgrids," in *Proc. Brazilian Power Electron. Conf. (COBEP)*, Nov. 2017, pp. 1–6.
[21] D. Dong, I. C. D. Boroyevich, W. Zhang, R. Wang, and P. Mattavelli, "Grid-interface bidirectional converter for residential DC distribution systems–Part one: High-density two-stage topology," *IEEE Trans. Power Electron.*, vol. 28, no. 4, pp. 1655–1666, Apr. 2013.
[22] R. M. S. Filho, P. F. Seixas, P. C. Cortizo, L. A. B. Torres, and A. F. Souza, "Comparison of three single-phase PLL algorithms for UPS applications," *IEEE Trans. Ind. Electron.*, vol. 55, no. 8, pp. 2923–2932, Aug. 2008.

Thiago R. Oliveira (M'12) was born in Belo Horizonte, Minas Gerais, Brazil. He received the B.Sc. and M.Sc. degrees in electrical engineering from the Federal University of Minas Gerais (UFMG), Belo Horizonte, Brazil, in 2008 and 2011, respectively.

He is currently an Assistant Professor with UFMG. His main research interests include dc power distribution, hybrid microgrids, and highly efficient converter design.

Waner Wodson A. G. Silva (SM'18) was born in Montes Claros, Minas Gerais, Brazil. He received the bachelor's degree in electrical engineering from the Faculdades Santo Agostinho, Montes Claros, Brazil, and the M.Sc. from the Federal University of Minas Gerais, Belo Horizonte, Brazil, in 2011 and 2013, respectively.

He is currently an Assistant Professor of power electronics and embedded systems with the Federal University of Itajuba, Itabira Campus, Brazil. His research interests include power electronic applications in renewable energy, energy storage, and embedded systems.

Seleme I. Seleme, Jr. received the B.S. degree in electrical engineering from Escola Politecnica, Sao Paulo, Brazil, the M.S. degree in electrical engineering from Federal University of Santa Catarina, Florianopolis, Brazil, and the Ph.D. degree in control and automation from the Institut National Polytechnique de Grenoble, Grenoble, France, in 1977, 1985, and 1994, respectively.

In 2002, he spent a sabbatical leave with the Power Electronics Group, University of California, Berkeley, CA, USA. In 2015, he spent a sabbatical leave with the Institut National Polytechnique de Toulouse, Toulouse , France, where he developed research about decentralized control and capacitor voltage estimation techniques for modular multilevel converters. He is currently an Associate Professor with the Department of Electronic Engineering, Federal University of Minas Gerais, Belo Horizonte, Brazil. His main research interests include renewable energy systems, modular multilevel converters, and nonlinear control applied to power converters.

Pedro F. Donoso-Garcia was born in Lima, Peru. He received the bachelor's degree in electrical engineering from the Federal University of Rio Grande do Sul, Porto Alegre, Brazil, the M.Sc. degree from the Federal University of Minas Gerais (UFMG), Belo Horizonte, Brazil, and the Ph.D. degree from the Federal University of Santa Catarina, Florianopolis, Brazil, in 1981, 1986, and 1991, respectively.

He is currently a Full Professor with the Department of Electronic Engineering, UFMG. His research interests include high-efficiency power supplies, electronic ballasts, distributed energy-storage systems, and microgrids.